LAWRENCE
LIVERMORE
NATIONAL
LABORATORY

LLNL-TR-834690

VTO battery project FY22 Q2 quarterly report

J. Ye

May 3, 2022

Disclaimer

This work performed under the auspices of the U.S. Department of Energy by Lawrence Livermore National Laboratory under Contract DE-AC52-07NA27344.

Please DO NOT CUT/PASTE OVER THESE FIRST PAGE SECTIONS.

We are trying to preserve ongoing editing to this first page by the Program Manager's team.

Instead, just make any changes directly to this page as needed.

Task 1.10 – Three-Dimensional Printing of All-Solid-State Lithium Batteries (Jianchao Ye, Lawrence Livermore National Laboratory)

Project Objectives. The project has two primary objectives: (1) down select three-dimensional (3D) printing and post-processing approaches for SSE/cathode integration, and (2) understand battery failure mechanisms via *ex situ* and *in situ* characterization.

Impact. The adoption of thin separator layer, thick cathode structure, and metallic lithium anode will lead to EV batteries with a > 350 Wh/kg energy density for increased mileage per charge. The higher ionic conductivity with suppression of lithium dendrite growth will allow high CCD for fast charging applications. The improved electrode/electrolyte contact will increase battery cycle life for long-term service.

Approach. The technical approaches include advanced manufacturing based on 3D printing and related techniques, *ex situ* / *in situ* characterizations, and battery testing. Direct ink writing (DIW) 3D-printing techniques will be employed to fabricate thin-film SSEs (< 100 μm), gradient SSEs, and 3D interfaces for battery performance evaluation. Three approaches including sintering-free, hybrid, and co-sintering will be investigated. The knowledge obtained from these approaches is transferable and complementary to each technique.

Out-Year Goals. The long-term vision of the team is to 3D-print all components of the ASSLBs to facilitate the scale-up of ASSLB manufacturing. In this project, the team will tackle the issues emerging from integrating SSEs with electrodes. The project goal is to demonstrate a successful 3D-printing approach to integrate SSE into electrodes and show reasonable capacity retention (that is, > 80%) after 300 cycles at current density ≥ 1 mA/cm^2.

Collaborations. The team will work closely with a computational partner (Task 3.11 led by B. Wood) to better understand battery failure mechanisms and design new battery architectures and chemistries for performance improvement.

Milestones

1. Determine the polymer / $Li_{6.4}La_3Zr_{1.4}Ta_{0.6}O_{12}$ (LLZTO) interfacial chemistry effects on the total ionic conductivity and Li^+ transference number. (Q2, FY 2022; Complete)
2. Improve conductivity and strength of composite polymer electrolytes (CPEs). (Q3, FY 2022; On schedule)
3. Obtain porous co-sintered LLZTO-SSE/NMC/C electrolyte/cathode bilayer structure. (Q4, FY 2022; On schedule)

Progress Report

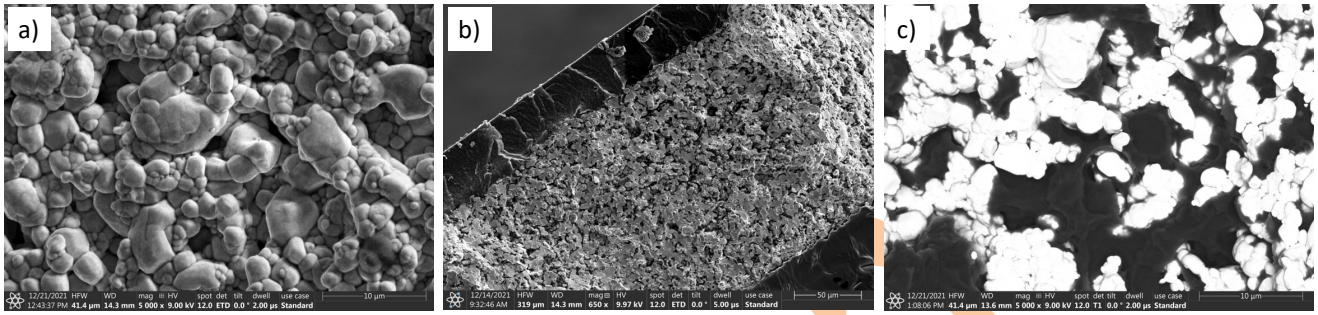

Figure 1. SEM images of a) pristine LLZTO film; b) SPE infilled LLZTO films, c) Backscattered electron image of the LLZTO/ SPE system.

In previous studies, it was found that the densification of printed LLZTO films by furnace sintering is challenging due to the low packing density of the green films and the severe Li loss issue at high sintering temperatures. Poor densification will lead to low ionic conductivity, and mechanical fragility and thus not ideal for direct application as ASSB separators. The team therefore investigated the possibility of a hybrid electrolyte using the porous LLZTO as scaffold and solid polymer electrolyte (SPE) as flexible and conductive filler, aiming at improving conductivity and cracking resilience. PEGDA/PEGMEA/PEO/LiTFSI SPE was chosen as the infilling polymer electrolyte based on previous studies on SPEs. **Figure 1** shows the SEM images of a pristine LLZTO porous film as well as the hybrid system after infilling and curing of corresponding monomers. Most of the pores were filled with the SPE, although gaps can be observed in the fracture surface, implying that the wetting between the pristine LLZTO and SPE may not be sufficiently well. The pristine porous LLZTO films show a poor room temperature ionic conductivity of 1.16 x 10^{-5} S/cm. After the LLZTO films are acid treated with H_3PO_4, the overall resistance decreases due to the removal of the surface contaminants such as Li_2CO_3 and thus the conductivity increases to 3.58 x 10^{-5} S/cm. By adding SPE in the pores of the LLZTO films, It is expected to introduce extra Li^+ transport channels and thus further improve the overall conductivity. As shown in **Table 1**, the total ionic conductivity of the SPE/infilled pristine LLZTO (SPE/LLZTO/SPE) is 1.27 x 10^{-5} S/cm, higher than SPE alone (7.1 x 10^{-6} S/cm). After removing the contributions from the SPE layers top and bottom of the SPE/LLZTO/SPE hybrid system, the conductivity of the SPE infilled pristine LLZTO layer is 2.5 x 10^{-5} S/cm, higher than pristine LLZTO film, but slightly lower than the acid treated LLZTO film only, which may be partially due to the gaps observed in **Figure 1**. The ionic conductivity at 60 °C, Li^+ transference number and critical current density values are also improved with the LLZTO scaffold as shown in **Table 1**.

Table 1. Ionic conductivity (σ_{Li}) at RT and 60°C, activation energy (E_a) at 60°C, transference number (t_{Li+}) at 60°C, and critical current density (CCD) at 60°C of the polymer SE and hybrid system (LLZTO/ Polymer) with different acid treatments conducted on LLZTO films.

Composition	Total σ_{Li} @ RT (mS/cm)	Total σ_{Li} @ 60°C (mS/cm)	E_a @ 60°C (eV)	t_{Li+} @ 60°C	CCD @ 60°C (mA/cm^2)
Polymer SE	0.0071±0.002	0.12	----------	0.24±0.03	0.13
SPE/ LLZTO/SPE	0.0127±0.0002	0.173±0.027	0.46	0.41±0.07	0.25±0.02
SPE/HCl- LLZTO/SPE	0.017±0.005	0.171±0.056	0.51	0.44±0.02	0.22±0.04
SPE/H_3PO_4-LLZTO/SPE	0.0076±0.0007	0.153±0.051	0.45	0.59±0.01	0.28±0.02

To remove a possible ion-blocking effect due to the presence of the surface Li_2CO_3 contaminant layer, different treatments using HCl acid and H_3PO_4 acid to either remove Li_2CO_3 or convert it into other Li species were carried out on the porous LLZTO films. **Figure 2** shows the XPS analysis of the pristine and acid treated LLZTO films. The La and Zr peaks in pristine LLZTO are very weak due to the existence of Li_2CO_3 surface

layer, in contrast, these peaks are observed for the acid treated LLZTO films. As expected, the surface of the acid treated film is decorated with either Cl^- from HCl or PO_4^{3-} species from H_3PO_4 (**Figure 2e-f**).

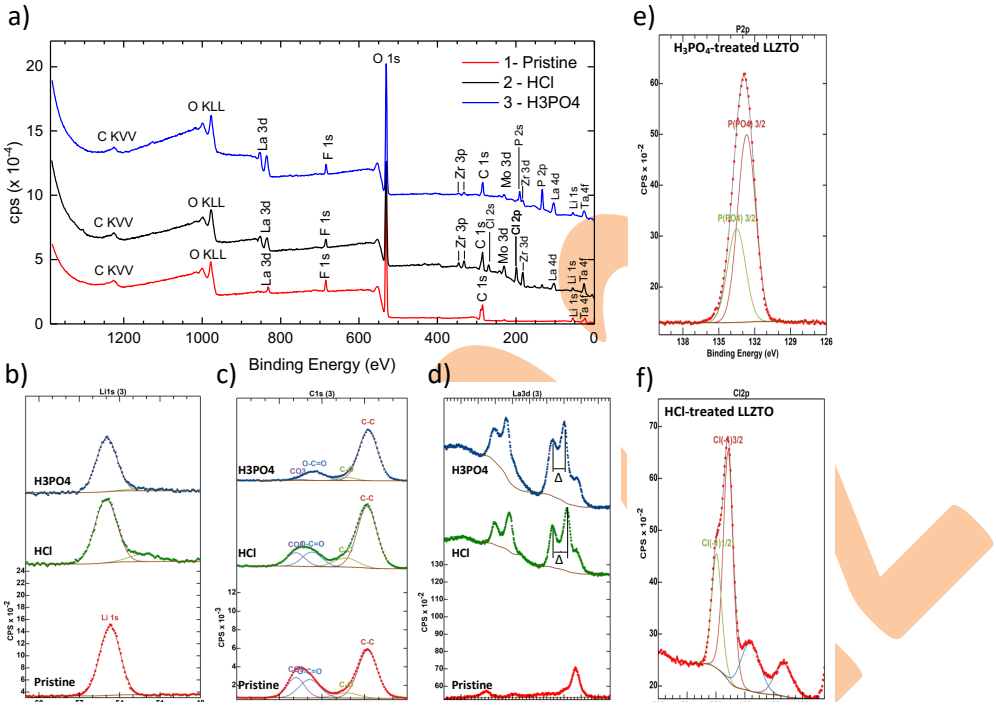

Figure 2. XPS survey scan of a) Pristine LLZTO film and acid treated LLZTO films, HCl and H_3PO_4; b) High resolution Li 1s XPS spectra; c) High resolution C 1s XPS spectra; d) High resolution La 3d XPS spectra; e) High resolution P 2p XPS spectra; e) High resolution Cl 2p XPS spectra.

Figure 3a-c shows the chronoamperometry (CA) plots and the EIS plots before and after DC polarization. Decreased charge transfer resistances were observed after Li plating/stripping, implying an improved interfacial contact between Li and SPE in Li/SPE/LLZTO/SPE/Li. The transference numbers were further increased especially for the H_3PO_4 treated sample, up to 0.59 (**Table 1**). The CCD value for HCl treated LLZTO film is lower than that of the pristine film (0.22 mA/cm^2 vs 0.25 mA/cm^2), while H_3PO_4 treatment

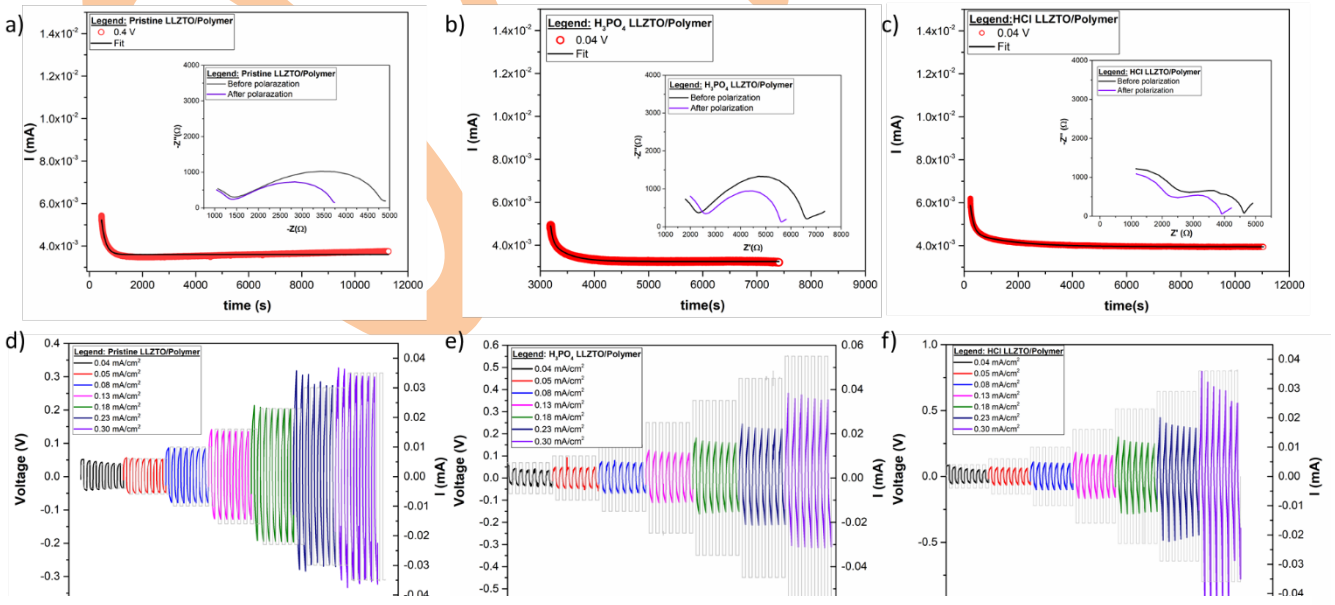

Figure 3. a)-c) DC polarization curves for determining the Li^+ transference number under an applied voltage of 0.04 V at 60°C. a) Pristine LLZTO film; b) H_3PO_4 treated films; c) HCl treated film. The inset shows the impedance taken just before and immediately after the DC polarization experiment. The curves were fitted with a decay function and the steady state at the end of the curve was extrapolated. d)-f) Voltage vs time plots of plating-stripping at different current densities. d) Pristine LLZTO film; e) H_3PO_4 treated films; f) HCl treated film.

slightly increases the CCD to 0.28 mA/cm^2. However, the total ionic conductivity of H_3PO_4 treated LLZTO sample after SPE infilling is the lowest.

To simplify the 3D interface problem, the team designed different control experiments to compare the cycling behaviors of four model Li symmetric cells: 1) Li|SPE|Li; 2) Li|SPE|infilled-LLZTO|SPE|Li; 3) Li|SPE|LLZTO-1100C|Li; 4) Li|SPE|LLZTO-1100C|SPE|Li. The first two cell configurations (1 and 2) (**Figure 4a-b**) show symmetric voltage profiles, suggesting Li^+ transport along both directions is similar. This symmetry seems to be intuitive for a symmetric cell setup. However, when the SPE infilled LLZTO layer is replaced with a well densified LLZTO pellet, e.g., in the configuration of Li|SPE|LLZTO-1100C|SPE|Li (**Figure 4c**), the team observed an asymmetric cycling behavior. The overpotential in the second half cycles increases more rapidly than the opposite direction. This abnormal asymmetry in a symmetric cell is still a mystery. Given the only difference between the above two setups (LLZTO infilled SPE and LLZTO/SPE) is that Li^+ ions can transport in both polymer and LLZTO channels in the infilled LLZTO case, versus Li^+ ions must transport from polymer to LLZTO and from LLZTO to polymer in the dense LLZTO case, the team suspect that the ion transport via LLZTO/SPE interface is the origin of this asymmetric behavior. In fact, in an SPE asymmetric cell using a densified LLZTO pellet stacked with only one SPE film (**Figure 4d**), the similar asymmetric behavior is observed, where Li^+ transport in the direction of LLZTO to SPE becomes much more difficult at current densities of 0.13 mA/cm^2 or above. The observed accelerated degradation is found in Li|SPE|Li, Li|SPE|LLZTO-1100C|Li, and Li|SPE|LLZTO-1100C|SPE|Li, but not in Li|SPE|infilled-LLZTO|SPE|Li. The

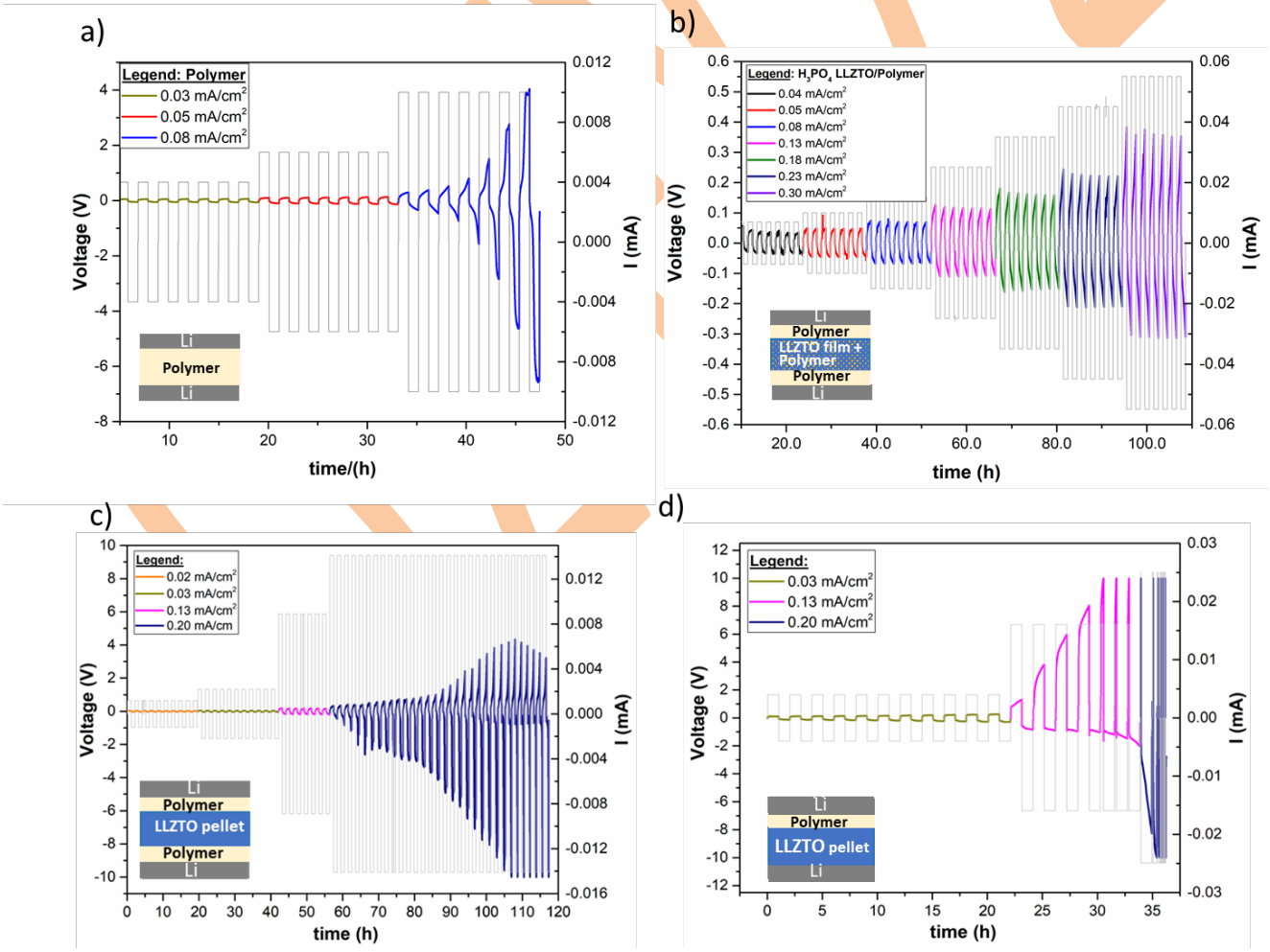

Figure 4. Voltage vs time plots at 60°C of the four model systems assembled to understand the conductivity differences: a) single SPE layer; b) SPE infilled porous LLZTO film (H_3PO_4 treated); c) stacked SPE, densified LLZTO pellet (H_3PO_4 treated) and SPE; d) stacked SPE and densified LLZTO pellet (H_3PO_4 treated) bilayers. Their corresponding cycling stability tests showing symmetric and asymmetric cycling behaviors.

observations suggest an advantage in using the SPE infilled LLZTO, while detailed understanding of the degradation mechanism is still needed. Possible explanations to be scrutinized in future work include: 1) charge accumulation and clogging at the LLZTO/SPE interface due to the sluggish charge transport from LLZTO to SPE; 2) Polymer/Li interface degradation at high voltages. To further enhance the performance of the hybrid electrolyte, the ionic conductivity of SPEs, and their compatibility with LLZTO shall be improved, which will be the next research focus area.

Patents/Publications/Presentations

Publications

- Hammons, J.; Espitia, J. A.; Guzman, E. R.; Shi, R.; Meisenkothen, F.; Wood, M.; Ceron, M. R.; Ye, J. Pore and Grain Chemistry during Sintering of Garnet-type Li6.4La3Zr1.4Ta0.6O12 Solid-state Electrolytes. *J. Mater. Chem. A* **2022**.